Characterization and Charge Transfer Mechanism of PIN–CdSe Nanocomposites

Hatice Ozkazanc
Department of Chemistry, Kocaeli University, 41380 Kocaeli, Turkey

This paper reports structural, thermal, and temperature-dependent dielectric properties of polyindole–cadmium selenide (PIN–CdSe) nanocomposites. PIN and its nanocomposites were synthesized via *in situ* chemical oxidative polymerization method. Samples were characterized by Fourier transform infrared spectroscopy (FT-IR), X-ray diffraction (XRD), scanning electron microscopy with energy dispersive X-ray (SEM/EDX), atomic force microscope, differential scanning calorimetry (DSC) and thermogravimetric analysis (TGA). Dielectric properties were analyzed as a function of temperature. FT-IR spectroscopy indicated that both N—H and aromatic C=C bonds were affected more by doping process. Significant structural differences were observed in XRD and SEM analyses of PIN and its nanocomposites. Both XRD and DSC measurements revealed that crystallinity of the PIN increases to a certain degree with increasing doping level. Thermogravimetric analysis showed that addition of CdSe decreased degradation temperature of the PIN. Conductivity measurements investigated by universal power law indicated that the charge transport mechanism of all the samples is consistent with correlated barrier hopping model. POLYM. COMPOS., 00:000–000, 2015.

INTRODUCTION

Polyindole (PIN) is an electroactive polymer with applications in diverse fields such as electronics, pharmacology, electrochromic devices, anticorrosion coatings, electro-catalysis, diverse sensors and battery electrodes. It has a high thermal stability, high redox activation, and low toxic efficiency compared to other conducting polymers such as polyaniline and polypyrrole [1, 2]. PIN which is among aromatic compound based polymers has been a subject of a considerable research interest in recent years [2–4]. The primary reason for this interest lies in its similar structure to other conducting polymers such as polypyrrole, polycarbazole, and poly(para-pehenylene). All these conducting polymers have both benzene ring and pyrrole ring [5, 6]. Studies on producing new materials with interesting physical and chemical properties mainly focus on blends and composites of the PIN [7–10].

Experimental parameters such as temperature, oxidant and acid types, doping material, and molar ratio of oxidant to monomer used in the synthesis of the polymeric composites have a direct effect on their physical and chemical properties. Significant results have been reported on PIN based nanocomposites in recent years. Costa et al. [2] have determined that Al-MCM-41 doping process increases the thermal stability and conductivity of the PIN. Joshi and Prakash [11] showed that PIN/Au nanocomposites may be used in the production of nanosized organic devices. Zhijiang and Chengwei [12] have reported that zinc/polyindole batteries exhibited desirable charge and discharge properties.

To the best our knowledge, PIN–CdSe nanocomposites have not previously been reported in literature as CdSe as an inorganic doping material has found impressive applications such as photoconductive devices, solar cells, sensors, and transistors [13, 14]. The porous structure of PIN leads to efficient diffusion paths for electrolyte ions, that would significantly promote the insertion of the ions and raise utilization rate of electrode materials [15, 16]. Also, the reduction of the conductivity of PIN by doping process can enable using PIN–CdSe nanocomposites for electrorheological applications, such as actuators, high voltage power supplies, and control circuits [17, 18].

The first part of this study concerns with the synthesis of PIN and its composites. They have been prepared by *in situ* chemical oxidative polymerization using $FeCl_3$ as an oxidizing agent and keeping the $FeCl_3$ to indole molar ratios as 3:1 and 3:2. Second part reports structural and thermal properties of the samples. Final part explains the charge transport mechanism of all samples through temperature-dependent dielectric measurements.

EXPERIMENTAL

Materials

Indole, anhydrous iron(III) chloride ($FeCl_3$), chloroform ($CHCl_3$) were supplied by Merck (Germany). CdSe

Correspondence to: Hatice Ozkazanc; e-mail: kiremitci@kocaeli.edu.tr
Contract grant sponsor: Research Fund of the Kocaeli University; contract grant number: Project No 2013/23.
DOI 10.1002/pc.23503
Published online in Wiley Online Library (wileyonlinelibrary.com).

(average particle size: 100 nm) was purchased from Aldrich. Indole and other chemicals were used directly without further purification.

Preparation of Polyindole

Two different molar ratios of $FeCl_3$ to indole (3:1 and 3:2) were used in the synthesis of PIN. 0.048 mol of $FeCl_3$ was mixed with 0.016 and 0.032 mol indole with molar ratios of 3:1 and 3:2 separately in 30 mL $CHCl_3$ for 30 min. In order to increase the volume of the solution to 100 mL, additional 40 mL $CHCl_3$ was added. $FeCl_3$ was then added dropwise into the indole solution in ice bath and stirred for 5 h. Polymerization process was performed under argon atmosphere. Precipitates obtained were filtered and washed with 100 mL $CHCl_3$ and 2 × 100 mL hot de-ionized water, respectively. Brown-colored PIN samples were obtained after drying at 70 °C under vacuum for 48 h.

Preparation of Nanocomposites

Indole solutions were prepared in $CHCl_3$ according to molar ratios and time intervals mentioned above. CdSe (0.522 and 1.044 mmol), which was stirred in 40 mL $CHCl_3$ and ultrasonic bath for 1 h to reduce aggregation of CdSe nanoparticles. 40 mL $CHCl_3$ was then added into these solutions. After stirring for 30 min in ice bath, $FeCl_3$ (dissolved in $CHCl_3$) was added dropwise into the mixtures and polymerization process was started. This process continued under argon atmosphere and in ice bath for 5 h. Filtering, washing and drying were carried out for samples as outlined above. Brown-colored PIN–CdSe composites were obtained after polymerization process.

PIN, prepared with 3:1 molar ratio was named as sample A and its composites, containing 0.522 and 1.044 mmol CdSe, were named as samples B and C, respectively. PIN, prepared with 3:2 molar ratio was named as sample D and its composites, containing 0.522 and 1.044 mmol CdSe, were named as samples E and F, respectively. Samples will be quoted as A, B, C, D, E, and F for the remainder of this paper.

Instruments and Characterizations

FT-IR (Shimadzu FT-IR 8201 spectrophotometer) measurements were taken between 4,000 and 400 cm^{-1} using the KBr pellet method. X-ray (RIGAKU MINIFLEX-2 Diffractometer with Cu Kα radiation) diffraction patterns were collected in 2θ range of 10°–80° with scanning step width of 0.02 deg (2θ)/min. Thermal properties were determined by DSC (Perkin Elmer DSC 4000) between 0 and 400 °C with 20 °C/min heating rate and TGA (Perkin Elmer TGA 4000) between 30 and 1,000 °C with 10 °C/min heating rate both under nitrogen atmosphere. Surface morphologies of the samples were examined using a SEM–EDX (JOEL 50 A) with micrographs taken at 20 kV and a Nanomagnetics ezAFM with tapping mode.

Pellets with 13 mm diameter were prepared under a 10 MPa of hydraulic pressure. Each of the pellets weighted approximately 0.1 g, and their thickness varied between 0.55 and 0.75 mm. Copper plates with 13 mm diameter and 2 mm thickness were used as electrodes. An LCR meter (Sourcetronic 2826A) was used for dielectric measurements at a range of 10 kHz–1 MHz frequency and 300–400 K temperature under vacuum ($\sim 10^{-3}$ Torr). Temperature adjustment was made by a Lakeshore 335 temperature controller. The alternating current (ac) conductivity was calculated from $\sigma_{ac} = \omega C_P d \tan\delta / A$, $\sigma_{ac} = \frac{\omega C_P d \tan\delta / A}{A}$ where ω is the angular frequency, C_P is the capacitance, d is the sample thickness, tanδ is the dielectric loss factor, and A is the electrode area.

RESULTS AND DISCUSSION

Characterization

FT-IR spectra of CdSe and samples A, B, C, D, E, and F are shown in Fig. 1. The peaks at 3,448 and 1,630 cm^{-1} for CdSe are assigned to O—H stretching and OH of water [19, 20]. The FT-IR spectrum of the PIN matches well with results reported in literature. Some of the observed characteristic bands of PIN samples and their composites are given Table 1. The most pronounced shift as a result of the doping was observed at 1,600 cm^{-1} (C═C bond) for both 3:1 and 3:2 molar ratios of the PIN. Moreover, intensity of the N—H stretching band increases with CdSe doping. These results suggest that the doping process affects both C═C and N—H bonds more.

When investigating the mechanism of interaction between polymers and metal ions, one should note that role of Cd and Se ions in the polymer as well as the presence of other metal ions is crucially important as some metal ions may have originated from the oxidant and may not move away from the structure despite the washing process. EDX spectra given in Fig. 2 show the existence of Fe ions arising from the oxidant ($FeCl_3$) used in the synthesis of the samples. It also shows that the nanocomposites (samples B, C, E, and F) contain different amounts of CdSe.

The effect of the doping process is also observed in XRD patterns of the samples (Fig. 3). The diffraction patterns of PIN and CdSe match well with the results reported previously. The peaks at 24.00°, 25.52°, 27.24°, 35.32°, 42.16°, 45.98°, 49.06°, 49.88°, and 50.86° are attributed to (100), (002), (101), (102), (110), (103), (200), (112), and (201) crystal planes, respectively [7, 10]. The peaks at 19.10° and 26.14° for sample A and the peaks between 15° and 30° for sample D are the characteristic peaks of the PIN in amorphous form. The new peaks at the range of 30°–50° for all composites indicate the existence of CdSe [19, 22, 23] in the polymer matrix and indicate an increased degree of crystallinity of the PIN.

 DOI 10.1002/pc

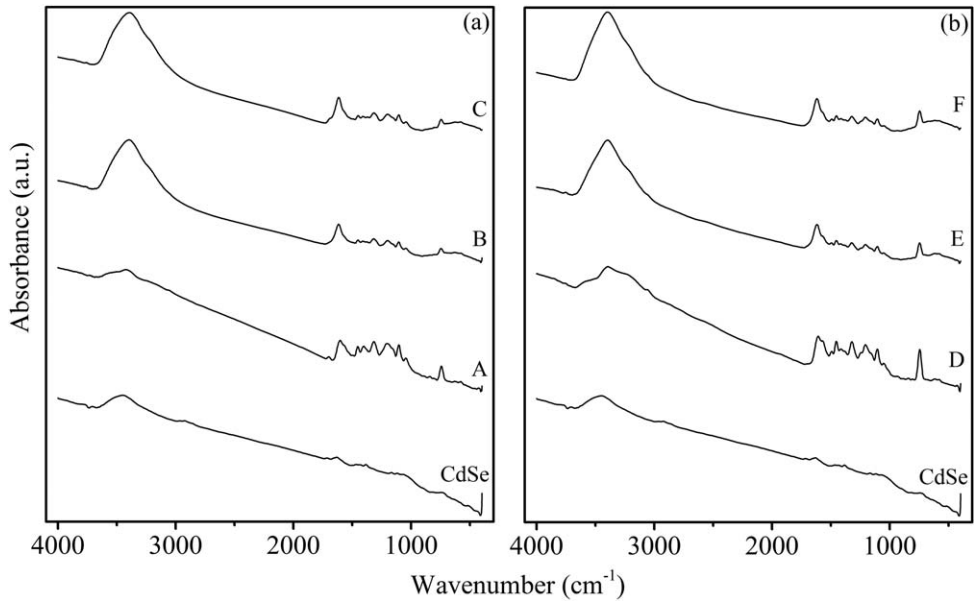

FIG. 1. FT-IR spectra of (a) 3:1 PIN and (b) 3:2 PIN and their nanocomposites.

Morphology

In the micrograph taken at ×1k magnification in Fig. 4a, it is seen that CdSe is in agglomerate structure due to high surface tension. These agglomerate structures have various sizes and geometries. Also, much smaller sized agglomerate structures are seen on big agglomerate structures. These small sized agglomerate structures can be seen more clearly in the micrograph with ×15k magnification (Fig. 4b). As can be seen in Fig. 4b, the average size of the smallest agglomerates that can be measured are about 175 nm. Agglomerate structures are seen more clearly in AFM phase images (Fig. 5). Smaller sized agglomerate structures can also be seen on big agglomerate structures here (Fig. 5a). The sizes of these small agglomerate structures, which were examined by AFM, are between 70 and 300 nm (Fig. 5b). These are quite in accordance with SEM results. Therefore, it can be said that powder CdSe nanoparticles are lower than 100 nm.

In order to reduce the aggregation and obtain better dispersion in the polymer, CdSe nanoparticles were stirred for 1 h in chloroform inside ultrasonic bath as mentioned in experimental part.

Microstructural differences between PIN and its composites prepared with the molar ratios of 3:1 and 3:2 are clearly seen in Fig. 6. The most significant difference is the pores which can be seen in the SEM images of PIN and composites with 3:2 molar ratios. This characteristic property of the PIN with porous structure can show itself in the surface images of the samples (D, E, and F) with higher monomer ratio. Furthermore, big particles beside small particles are seen in the micrographs of undoped PIN samples (Fig. 6a and d). Both particle size and the gap between the particles decrease significantly with increasing doping level (Fig. 6b, c, e, and f). Furthermore, particles with various dimensions and relatively lighter colors for the composites with the highest doping levels are shown in Fig. 6c and f. This can be due to a more pronounced crystalline phase.

FTIR, X-ray, and SEM–EDX analyses indicate that CdSe doping leads to structural differences which may affect thermal and electrical properties of the PIN.

TABLE 1. FT-IR band assignments of PIN samples and their nanocomposites.

	Band positions (cm^{-1}) and assignments[a]				
Samples	N—H bond	Vibration of $C_2{=}C_3$ aromatic bonds	Stretching mode of aromatic alkene	Vibration of C—N	Bending mode of aromatic alkene
A	3,425	1,602	1,452 and 1,205	1,317	742
B	3,394	1,616	1,448 and 1,201	1,317	746
C	3,390	1,614	1,448 and 1,199	1,315	744
D	3,394	1,608	1,454 and 1,207	1,321	746
E	3,394	1,618	1,454 and 1,207	1,323	746
F	3,400	1,618	1,454 and 1,207	1,323	746

[a]Refs. [2, 7, 8, 21].

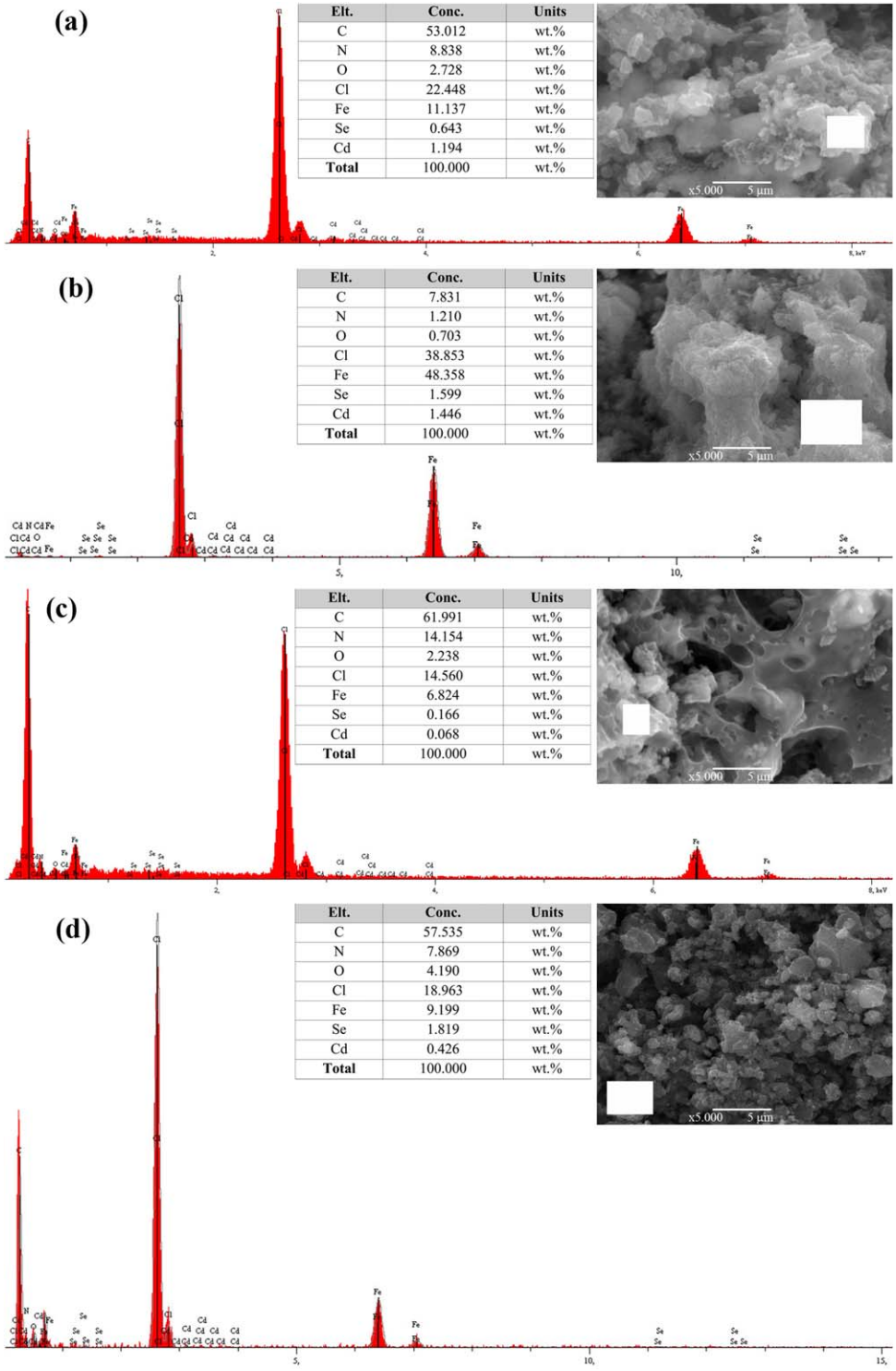

FIG. 2. SEM–EDX analyses of nanocomposites. (a) B, (b) C, (c) E, and (d) F. [Color figure can be viewed in the online issue, which is available at wileyonlinelibrary.com.]

Thermal Analysis

Figure 7 shows the DSC thermograms measured during the first heating of PIN samples and their composites. The endothermic peaks at around 110 and 150 °C for samples A and D are usually related to loss of moisture and evaporation of the solvent [8, 18]. These mass losses are also seen in TGA curves of the samples A and D (Fig. 8). The endothermic peak around 220 °C for all the composites is the characteristic melting peak of selenium [24]. The intensity increase in this peak with increasing

 DOI 10.1002/pc

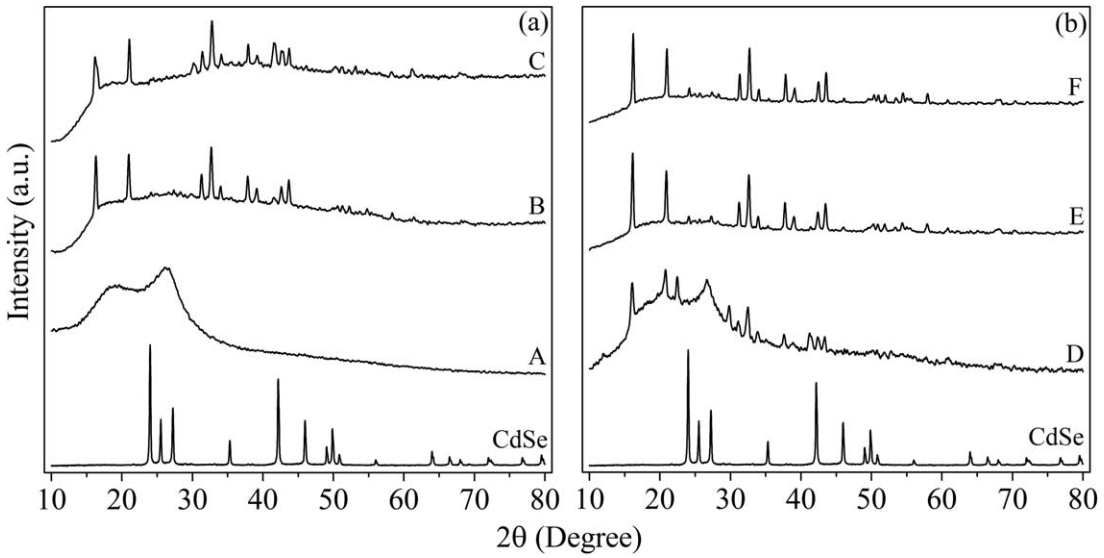

FIG. 3. X-ray diffraction patterns of (a) 3:1 PIN and (b) 3:2 PIN and their nanocomposites.

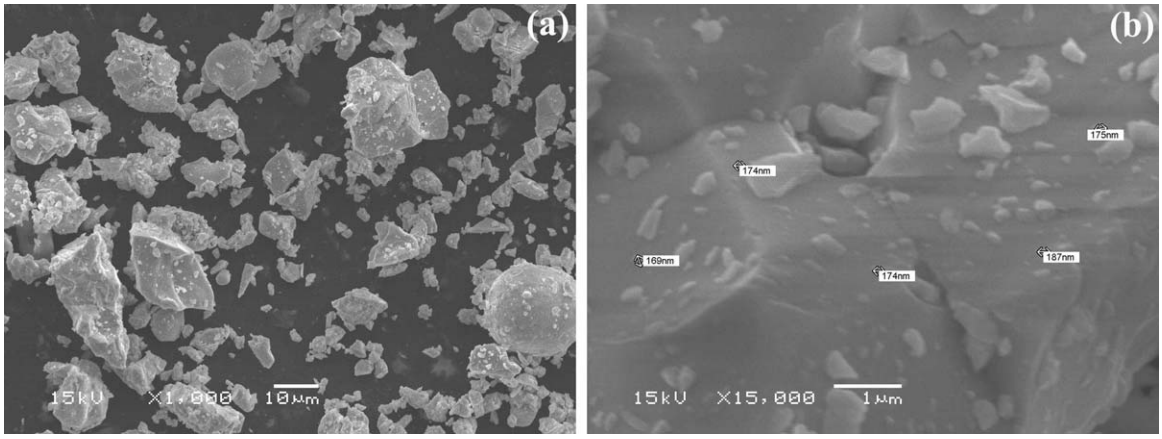

FIG. 4. SEM micrographs of CdSe nanoparticles at magnifications of (a) 1k and (b) 15k.

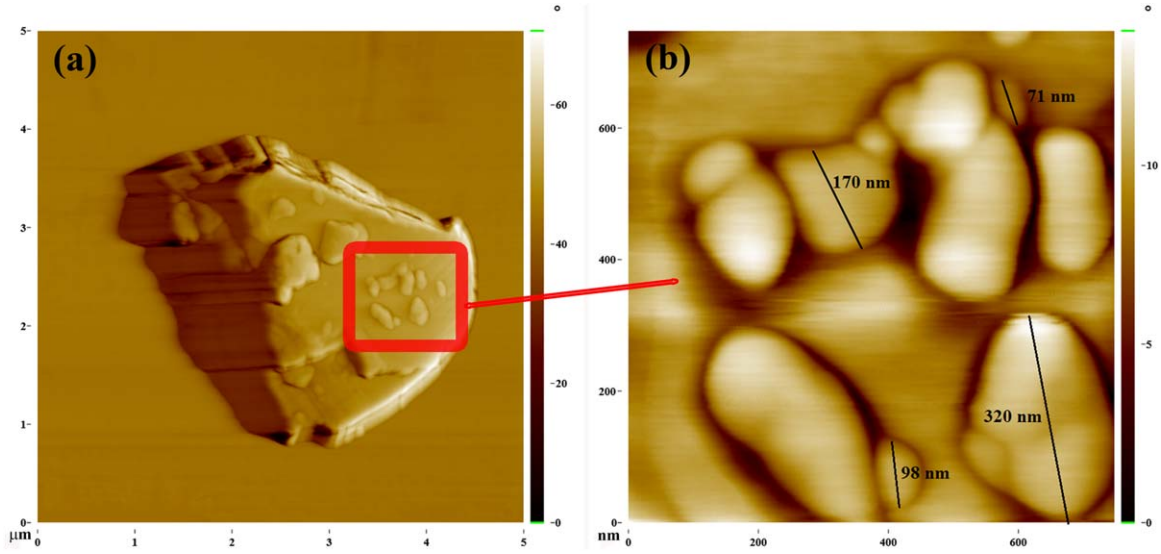

FIG. 5. AFM phase image of CdSe nanoparticles. [Color figure can be viewed in the online issue, which is available at wileyonlinelibrary.com.]

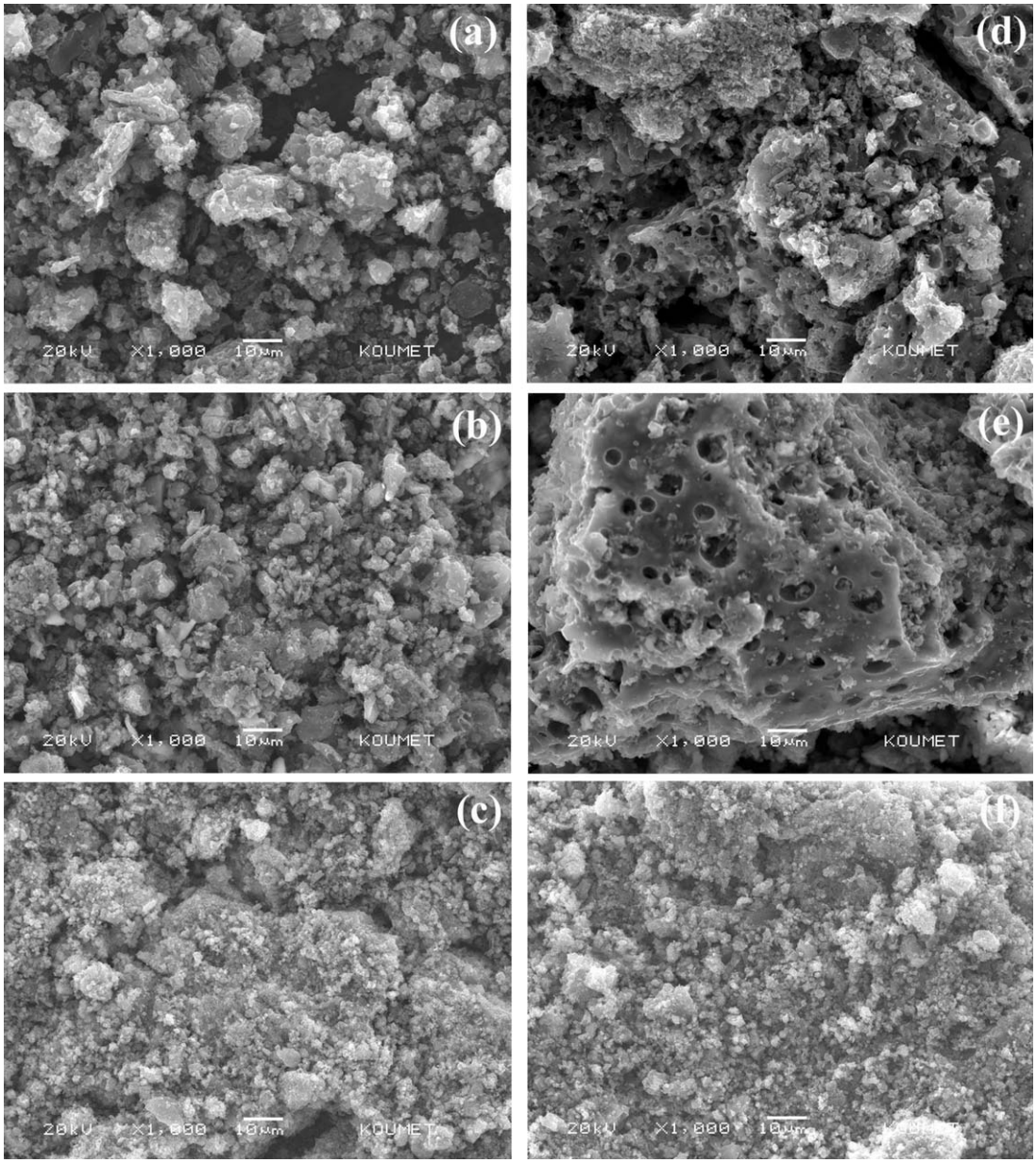

FIG. 6. SEM micrographs of samples (a) A, (b) B, (c) C, (d) D, (e) E, and (f) F.

Se is an indication that crystallinity increases to a certain degree as also confirmed by X-ray diffraction patterns.

TGA results indicated that the thermal stability of the composites is relatively lower than undoped PIN samples. This may be due to the fact that the metal ions have a relatively weaker coordination with the polymer chain rather than a strong interaction. At higher temperatures this interaction weakens further and the coordination between metal ions and the polymer breaks up. Hence, the composites degrade at lower temperatures compared to undoped PIN samples.

Charge Transfer Mechanism

The *ac* conductivity of amorphous semiconductor systems or polymers is usually investigated with the Power law:

$$\sigma_{ac} = A\omega^{s} \tag{1}$$

where A is a temperature dependent constant, ω is angular frequency and s is an exponent [25, 26]. There are various theoretical models such as Correlated barrier hopping (CBH), small polaron tunneling (SPT) and electron tunneling (ET). The frequency exponent 's' usually has values between 0 and 1 in these theoretical models. In these models, while 's' decreases with increase in the temperature for CBH model, 's' increases with increase in the temperature for SPT model. 's' is independent of temperature for ET model. The conduction mechanism is usually determined from variation of the frequency exponent 's' with temperature [26].

 DOI 10.1002/pc

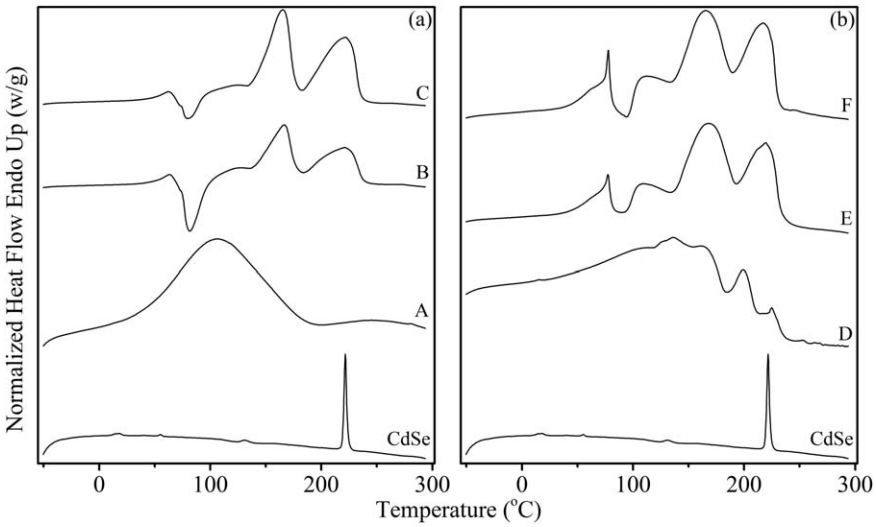

FIG. 7. (a) DSC thermograms of (a) 3:1 PIN and (b) 3:2 PIN and their nanocomposites.

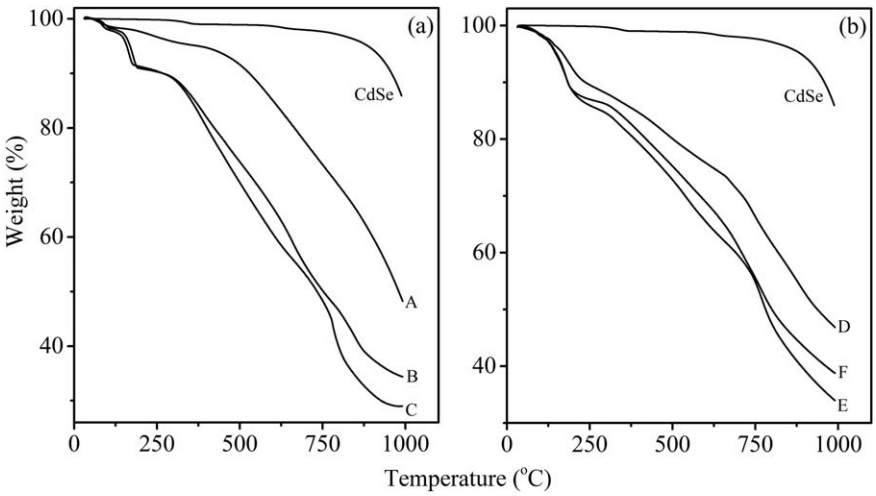

FIG. 8. TG curves of (a) 3:1 PIN and (b) 3:2 PIN and their nanocomposites.

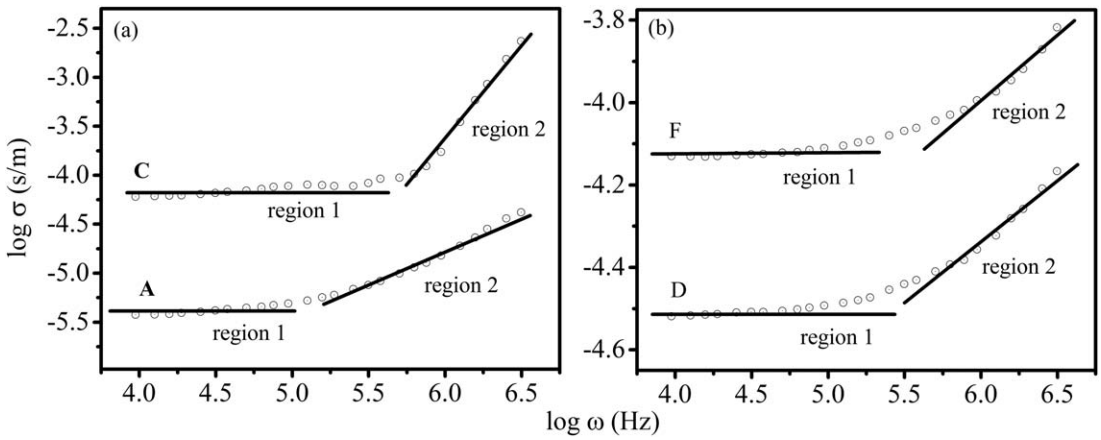

FIG. 9. Frequency dependence of ac conductivity of (a) samples A and C, (b) samples D and F at 300 K.

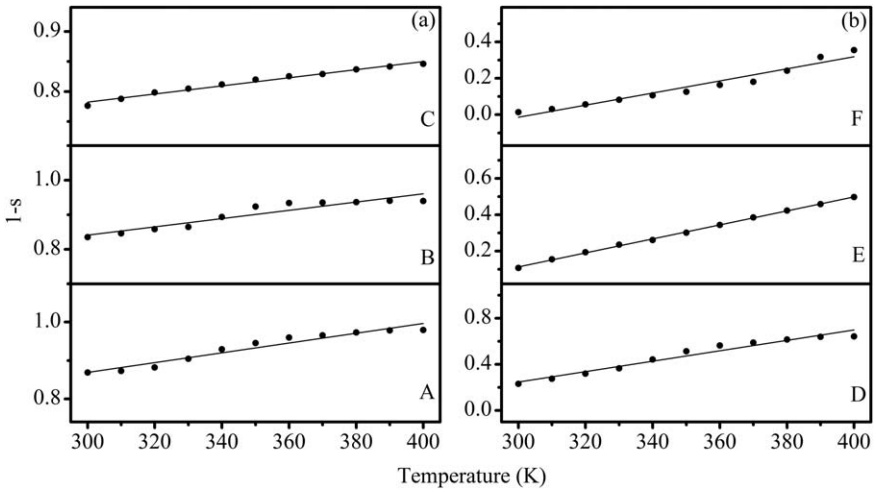

FIG. 10.VA. riation of 1-s vs. T for (a) 3:1 PIN and (b) 3:2 PIN and their nanocomposites.

As seen in Fig. 9, the *ac* conductivity is independent of frequency up to a certain value (region 1) and then increases with increases of frequency (region 2). The '*s*' values calculated from the slope of log σ vs. logω plot for region 2 at various temperatures are given in Table 2. As can be seen in Table 2, '*s*' values decrease with the temperature for all samples. Hence, by looking at these results, it is possible to say that the most suitable model is CBH (Eq. *2*):

$$s = 1 - \frac{6k_BT}{W_H + k_BT\ln(\omega\tau_0)} \quad (2)$$

where W_H is the activation energy, k_B is Boltzmann's constant ($k_B = 86.13\,\mu eVK^{-1}$), τ_0 is the relaxation time, and T is the temperature [27, 28]. For large values of W_H/k_BT,

TABLE 2. '*s*' values of the samples at different temperatures.

	Samples					
T(K)	A	B	C	D	E	F
	s' values					
300	0.131	0.165	0.224	0.769	0.892	0.986
310	0.127	0.154	0.212	0.725	0.845	0.969
320	0.118	0.141	0.202	0.681	0.806	0.944
330	0.096	0.135	0.195	0.635	0.765	0.917
340	0.071	0.106	0.188	0.557	0.739	0.894
350	0.054	0.076	0.180	0.487	0.698	0.874
360	0.040	0.066	0.175	0.437	0.656	0.836
370	0.034	0.065	0.171	0.411	0.615	0.820
380	0.027	0.064	0.163	0.384	0.577	0.758
390	0.022	0.059	0.158	0.362	0.541	0.683
400	0.020	0.060	0.154	0.357	0.502	0.645

TABLE 3. Activation energies of the samples.

Samples	W_H (eV)
A	0.40
B	0.43
C	0.76
D	0.11
E	0.13
F	0.15

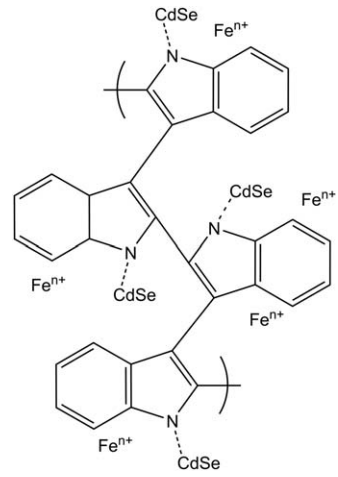

FIG. 11. Possible interaction mechanism ($n = 2$ or 3).

TABLE 4. Conductivity values of the samples.

	300 K		400 K	
Samples	10 kHz	1 MHz	10 kHz	1 MHz
	σ (S/m)			
A	5.12×10^{-4}	6.28×10^{-4}	2.87×10^{-3}	2.96×10^{-3}
B	3.50×10^{-5}	4.07×10^{-5}	6.28×10^{-4}	6.68×10^{-4}
C	4.50×10^{-6}	5.62×10^{-6}	9.53×10^{-5}	1.13×10^{-4}
D	4.56×10^{-6}	3.15×10^{-5}	3.90×10^{-5}	5.22×10^{-5}
E	1.32×10^{-6}	1.47×10^{-5}	1.94×10^{-5}	2.85×10^{-5}
F	4.77×10^{-7}	8.31×10^{-6}	2.34×10^{-5}	1.12×10^{-5}

DOI 10.1002/pc

's' is independent of frequency and hence, the slope of the graph of *1-s* vs. *T* would be equal to $6\ k_B/W_H$ (Fig. 10.Va). The best fit values of W_H are given in Table 3.

Activation energy needed for electron hopping for samples A, B, and C is higher than the samples D, E, and F. This may be due to the structural differences originating from the oxidant:monomer molar ratios as also seen in X-ray and SEM results. π-electrons and/or charged carriers may therefore follow different conducting path lengths.

As Table 4 shows, composites have higher activation energies when compared to their undoped PIN samples showing that the doping process decreases conductivity of the polymer. This may be due to the coordination between unpaired electrons of nitrogen atoms and CdSe. This coordination restricts the mobility of charged carriers. Decrease in the mobility of delocalized π-electrons interacting with the metal ions may be another reason. These conclusions are also supported by the FT-IR spectra, as explained above. The most probable interaction mechanism between polymer and metal ions is given schematically in Fig. 11 in the light of the results reported so far.

CONCLUSIONS

Structural, thermal, and dielectric properties of PIN–CdSe nanocomposites synthesized via *in situ* chemical oxidative polymerization have been reported for the first time.

FT-IR, XRD, and SEM/EDX analyses showed that the monomer concentration and doping process have significantly affected the morphology of the PIN. Thermogravimetric analysis indicated that the doping of CdSe decreased the thermal stability of the PIN. The *ac* conductivity behavior analysis by Power law showed that the charge transport mechanism of both PIN and its nanocomposites is consistent with correlated barrier hopping (CBH) model. Differences in the values of the activation energy of the PIN and its composites indicated that the doping process affected the lengths of the conductivity paths.

REFERENCES

1. M. Baibaraca, I. Baltog, M. Scocioreanu, S. Lefrant, and J.Y. Mevellec, *Synth. Met*., **159**, 2550 (2009).
2. M.B.G. Costa, J.M. Juárez, M.L. Martínez, J. Cussa, and O.A. Anunziata, *Microporous Mesoporous Mater*., **153**, 191 (2012).
3. M.T. Ramesan, *Polym. Compos*., **33**, 2169 (2012).
4. G. Rajasudha, L.M. Jayan, D.D. Lakshmi, P. Thangadurai, N. Boukos, V. Narayanan, and A. Stephen, *Polym. Bull*., **68**, 181 (2012).
5. J. Xu, J. Hou, W. Zhou, G. Nie, S. Pu, and S. Zhang, *Spectrochim. Acta A*, **63**, 723 (2006).
6. O. Soylu, S. Uzun, and M. Can, *Colloid Polym. Sci*., **289**, 903 (2011).
7. G. Rajasudha, H. Shankar, P. Thangadurai, N. Boukos, V. Narayanan, and A. Stephen, *Ionics*, **16**, 839 (2010).
8. Ö. Eraldemir, B. Sari, A. Gök, and H.İ. Ünal, *J. Macromol. Sci. A*, **45**, 205 (2008).
9. G. Nie, L. Qu, J. Xu, and S. Zhang, *Electrochim. Acta*, **53**, 8351 (2008).
10. L. Joshi, A.K. Singh, and R. Prakash, *Mater. Chem. Phys*., **135**, 80 (2012).
11. L. Joshi and R. Prakash, *Mater. Lett*., **65**, 3016 (2011).
12. C. Zhijiang and H. Chengwei, *J. Power Sources*, **196**, 10731 (2011).
13. M. Ali, W.A.A. Syed, M. Zubair, N.A. Shah, and A. Mehmood, *Appl. Surf. Sci*., **284**, 482 (2013).
14. S. Velumani, Sa.K. Narayandass, D. Mangalaraj, P.J. Sebastiana, and X. Mathew, *Sol. Energy Mater. Sol. Cells*, **81**, 323 (2004).
15. X. Ma, W. Zhou, D. Mo, B. Lu, F. Jiang, and J. Xu, *RSC Adv*., **55**, 3215 (2015).
16. W. Zhou, X. Ma, F. Jiang, D. Zhu, J. Xu,B. Lu, and C. Liu, *Electrochim. Acta*, **138**, 270 (2014).
17. O. Erol, H.I. Unal, and B. Sari, *Polym. Compos*., **31**, 471 (2010).
18. B. Sari, N. Yavas, M. Makulogullari, O. Erol, and H.I. Unal, *React. Funct. Polym*., **69**, 808 (2009).
19. P. Srivastava and K. Singh, *Adv. Mat. Lett*., **3**, 340 (2012).
20. S.A. Gawali and C.H. Bhosale, *Mater. Chem. Phys*., **129**, 751 (2011).
21. G. Rajasudha, A.P. Nancy, T. Paramasivam, N. Boukos, V. Narayanan, and A. Stephen, *Int. J. Polym. Mater*., **60**, 877 (2011).
22. M.N. Kalasad, M.K. Rabinal, and B.G. Mulimani, *Langmuir*, **25**, 12729 (2009).
23. W.S. Khan, C. Cao, F.K. Butt, Z. Ali, A. Ihsan, M. Tanveer, I. Aslam, G. Nabi, A. Rehman, T. Mahmood, and S. Hussain, *Mater. Lett*., **92**, 263 (2013).
24. M.F. Kotkata, A.E. Masoud, M.B. Mohamed, and E.A. Mahmoud, *Phys. E*, **41**, 640 (2009).
25. E. Ozkazanc, S. Zor, H. Ozkazanc, H. Y. Guney, and U. Abaci, *Mater. Chem. Phys*., **133**, 356 (2012).
26. S. De, A. De, A. Das, and S.K. De, *Mater. Chem. Phys*., **91**, 477 (2005).
27. F. Gmati, A. Fattoum, N. Bohli, and A.B. Mohamed, *J. Phys. Condens. Matter*, **20**, 125221 (2008).
28. E. Ozkazanc, S. Zor, H. Ozkazanc, and U. Abaci, *Polym. Eng. Sci*., **51**, 617 (2011).